WELDING TECHNOLOGIES.
SOLDERING

Properties of Ti−Ni Wire Welded Joints

A. R. Khismatullin[a], *, I. V. Kladov[a], O. V. Panchenko[a], and D. V. Kurushkin[a]

[a]Peter the Great St. Petersburg Polytechnic University, St. Petersburg, 197110 Russia

*e-mail: Khismatullin.Arthur@yandex.ru

Abstract—The welded joints of a nitinol (Ti−55.42% Ni) wire 2 mm in diameter are fabricated using a manual tungsten inert gas welding technology (TIG). The macro- and microstructure of the welded joints are investigated, bending tests are carried out, and the shape memory effect is evaluated.

Keywords: manual tungsten inert gas welding, nitinol, wire, shape memory effect, heat input

INTRODUCTION

Due to the needs of various industries, the process of new materials developing, which are focused on specific tasks, is constantly ongoing. Ti−Ni (nitinol) belongs to the class of materials with the shape memory effect. This class of materials tends to return their original geometry from a deformed state when exposed to heat or mechanical stress. This phenomenon of returning to its original form is called the shape memory effect [1].

Nitinol is used in various industries, such as automotive, aviation, biomedical, and the joining of this material is a challenging problem. Today, laser welding [2−5], friction stir welding [6, 7], resistance welding [8], and tungsten inert gas welding [9−11] are widely used to produce nitinol joints. This paper presents the study on the welding of wires, which are used as the basic component in the manufacturing of actuators and prostheses and can also be used for additive manufacturing.

The aim of this work is to study the welded joints of wires produced by TIG welding. The problems were to estimate the microstructure of the fusion zone, to perform bending tests, and to evaluate shape memory effect of the welded wires.

EXPERIMENTAL

The welding power source for manual tungsten inert gas welding Jasic TIG 315 P AC/DC was used to produce the welded joints. 15 welded joints were produced using the wire of a Ti−Ni alloy (Ti−55.42% Ni) with a diameter of 2 mm. The welding parameters (ID) are given in Table 1.

The fixture consisting of two overlapping copper plates was used for welding. One part of the wire was fixed with a clamp to the lower plate in the corner formed between the butt surface of the upper plate and the upper surface of the lower plate, while the second piece of the wire was fed manually. A schematic representation of the fixture is shown in Fig. 1. The fixture was designed to provide heat dissipation and co-directionality of the wires.

The fixture surfaces were preliminarily mechanically cleaned and degreased. The ends of the wires to be welded were cleaned on a grinder to remove the carbon coating and to produce smooth surfaces on the butt of the wires, after that they were degreased. Pure argon was used as a shielding gas.

The direct current electrode negative (DCEN) polarity arc mode was used. During experiments, a gradual change in current was performed. An arc was ignited on a copper substrate, after which the arc was gradually transferred to the butt joint.

Two joint samples of each welding parameters were selected from 15 welded joints, from which the cross
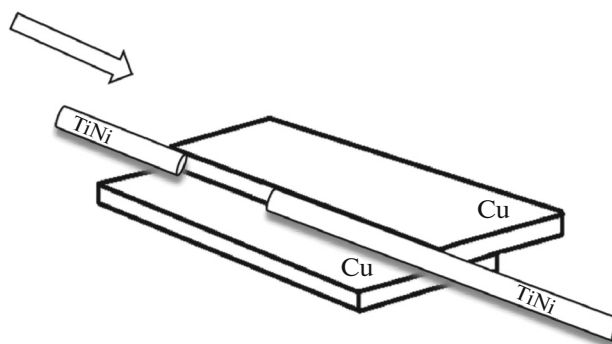

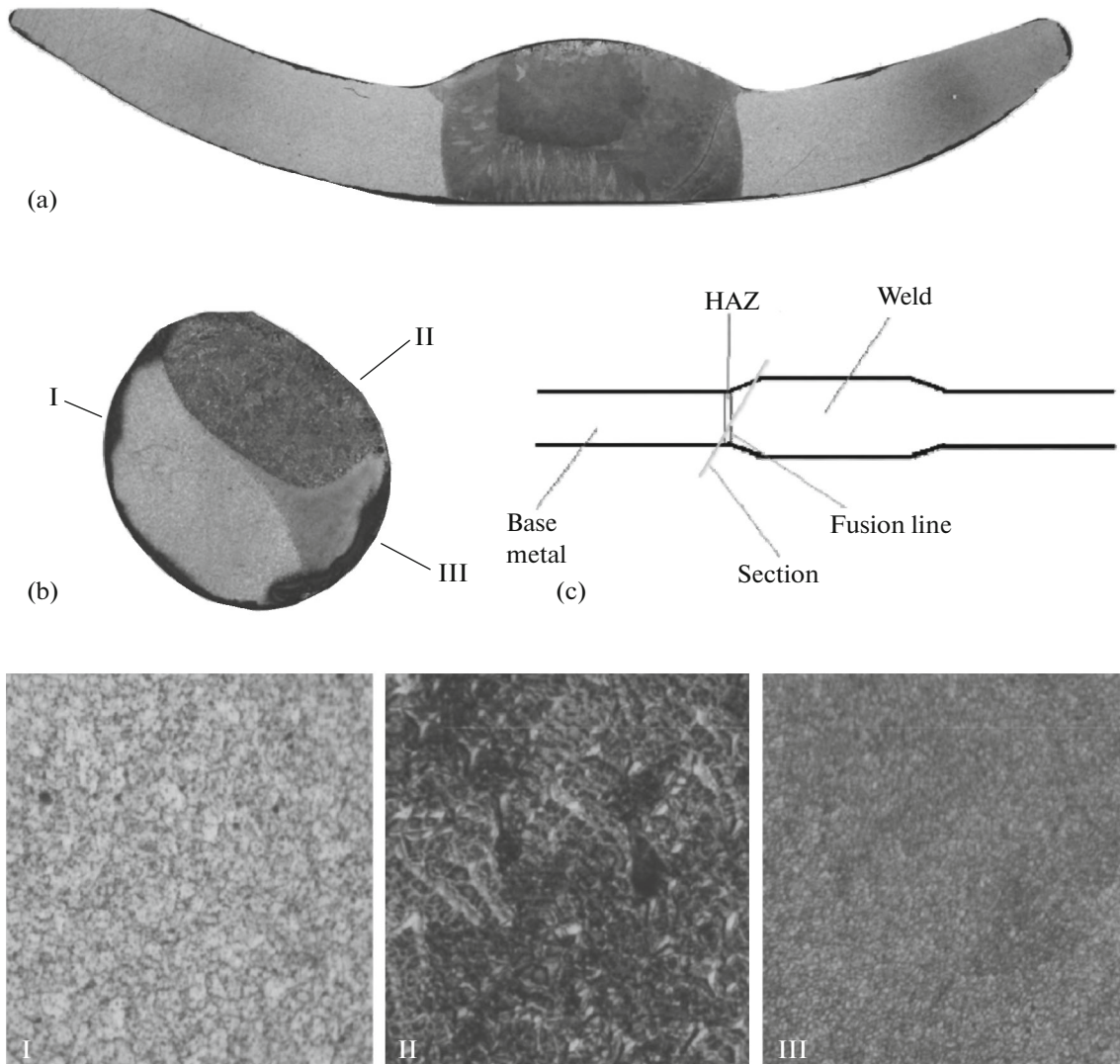**Fig. 1.** The layout of the wire on the substrate during welding.

Fig. 2. Photograph of the welded joint formed at a current value of 20A: (a) longitudinal section, (b) cross section, and (c) sectional diagram. Zone of the base metal (I), weld (II), and presumably HAZ (III).

sections of welded joints were made in the longitudinal and transverse directions (Figs. 2–6). Cross sections were polished using suspensions with a fraction in the following order: 6, 3, 1, 0.3 and 0.6 μm; the final stage was manual polishing using a mixture of a suspension of 0.4 μm and 3% hydrogen peroxide in a ratio of 4 : 1, respectively. The sections were etched in a mixture of nitric and hydrofluoric acid with water, $HF + HNO_3 + H_2O$, taken in a ratio of 1 : 4 : 5. The etching time was 15 s for the cross section and 30 s for the longitudinal section of each sample.

MICROSTRUCTURE

The microstructures of the longitudinal and transverse cross sections of the welded joint produced at a current of 20 A are shown on Figs. 2a, 2b, respectively.

Macrostructural analysis of the longitudinal section allowed us to recognize the base metal, the fusion boundary, and the weld. Grains with a clearly visible crystallization direction are observed in the welded joint. The heat-affected zone (HAZ) is supposed to be too small to be detected in macrographs; this may be due to the butt joint compression force of two parts of the wire during welding; this effect is observed for all three different IDs (Table 1).

Figure 2b shows the transverse cross-section of the welded joint with ID 1 parameters. This cross-section

Table 1. Welding parameters

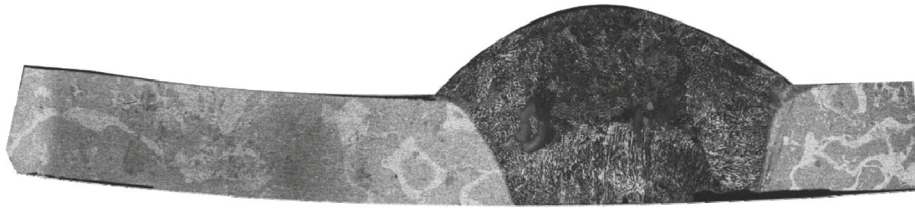|	ID 1	ID 2	ID 3
Current, A	20	30	40

Fig. 3. Longitudinal section of the welded joint formed at a current of 30 A.

Fig. 4. Cross section of the welded joint formed at a current of 30 A.

is made close to the fusion boundary at an angle of 20° (the cross-section scheme is shown in Fig. 2c) in order to capture the base metal, the HAZ, and the welded joint in one macrograph. Three zones can be visually recognized: the base metal zone (see Fig. 2, I), the weld metal zone (see Fig. 2, II), and heat affected zone (see Fig. 2, III). The base metal and weld metal zones are crystallized in the grain form morphology.

Figure 3 shows the longitudinal cross section of a welded joint obtained at the welding current of 30 A. In the weld zone, the metal crystallized in the form of dendrites, the growth of which is oriented from the weld pool boundaries to the center due to the temperature gradient. The base metal zone has identical microstructure in comparison to the longitudinal section that was previously described for a current of 20 A. Apparently, the light spots in Fig. 3 are the etching defects. The HAZ was not visually detected, and the welded zone can be recognized.

The weld metal has a dendritic microstructure (see transverse cross-section in Fig. 4).

The metal produced with a welding current of 40 A (ID 3) can be described similarly to the previous one (30 A), see macrograph in Fig. 5. Transverse cross-
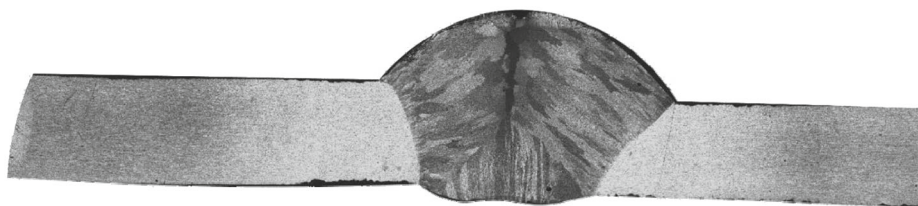

Fig. 5. Longitudinal section of the welded joint formed at a current of 40 A.
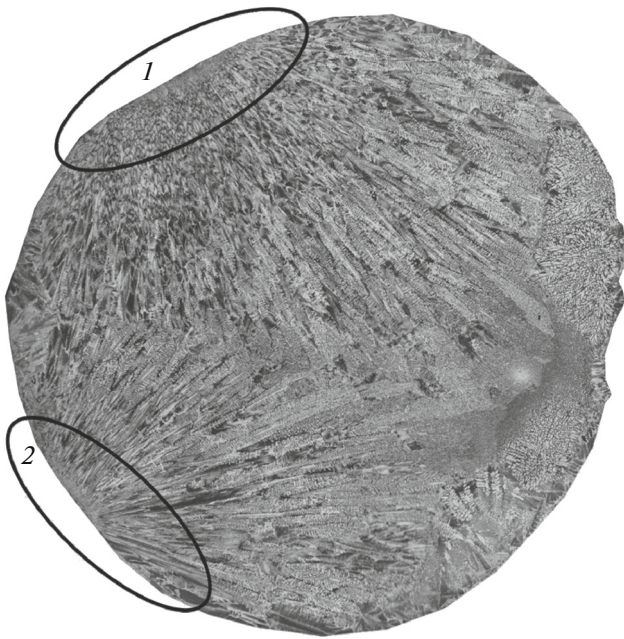
Fig. 6. Cross section of the welded joint formed at a current of 40 A: *1* and *2*, contact zones between the wire and the copper substrate.

Fig. 7. Setup of the wire bending assessment system.

section is shown in Fig. 6. The weld metal has a dendritic structure. The zone of contact between the wire and the copper substrate can be recognized due to the difference in the crystallite lengths (see regions 1, 2 in Fig. 6).

It can be concluded that the shape of crystallites in the welded metal depends on the welding current (heat input). In this case, the current above 20 A leads to formation of dendrites in the weld metal.

PLASTICITY

Bending tests of the welded wires were carried out. The experiment was constructed as follows: a wire was pressed against a 6-mm steel bar with a vice so that a weld was located at a distance of 1−2 mm from the point of wire−bar contact. The wire was then bent by hand until fracture or an angle of 90° to the vertical. The bending angle was measured with a protractor accurate to 0.5°. The setup is shown in Fig. 7.

The test results for each ID samples are presented in Table 2. The results give the maximum possible bend angles to failure. The best result was obtained for the ID 1 welding parameters, in which the metal was crystallized in the grain morphology.

SHAPE MEMORY EFFECT AFTER MANUAL ARGON ARC WELDING

After bending tests, one sample of the welded joint was selected from all three welding parameters; these samples were then bent to the following bending
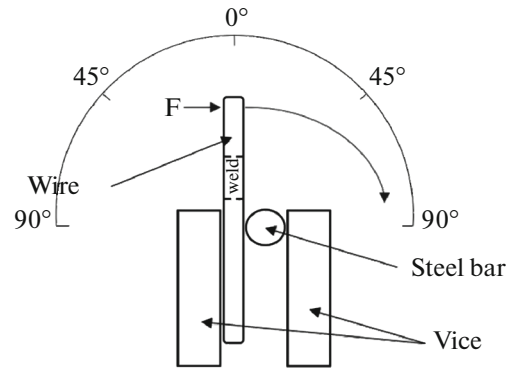
angles, in accordance with the minimum values from Table 2: 90°, 60° and 30° for 20, 30, and 40 A, respectively. Then the samples were heat treated at 150°C for 50 min. Figure 8 shows the wires welded joints photograph before bending (see Fig. 8a), after bending (see Fig. 8b), and after heat treatment (see Fig. 8c). A visual assessment of the wires shape after heat treatment indicates the presence of a shape memory effect due to the following fact: the tested zone around the weld was deformed and completely rebuilt. This result was observed for all samples from the experiment.

Thus, regardless of the welding parameters, the shape memory effect is retained if the maximum wire bend angle is limited.

CONCLUSIONS

(1) Welding conditions for achieving high plasticity of welded joints while maintaining the shape memory effect were developed (current of 20 A, high-purity argon protection, DCEN).

(2) The evaluation of the microstructure of welded joints obtained with various welding parameters indicates a direct relationship between the shape of crystallites and the welding current (heat input). For example, a decrease in the heat input promotes grain morphology in the metal microstructure, and an increase in the heat input promotes the formation of a dendritic (unfavorable) structure. These results are in accordance to the results of plasticity tests.

Table 2. Results of plasticity tests

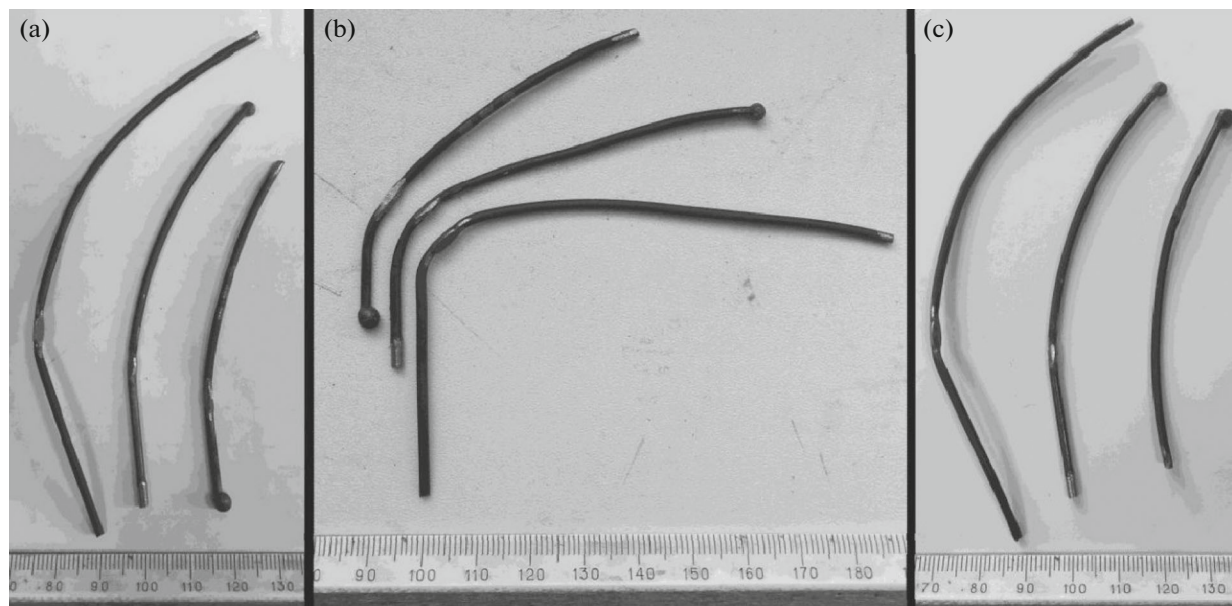| Current, A	20	30	40
Experiment 1	90°	80°	40°
Experiment 2	90°	60°	30°
Experiment 3	90°	90°	35°

Fig. 8. Evaluation of the shape memory effect: (a) before bending, (b) after bending, and (c) after heat treatment.

(3) The evaluation of the shape memory effect indicates preservation of this property in the welded wires regardless of the welding conditions.

REFERENCES

1. K. Ootsuka, K. Simudzu, Yu. Sudzuki, et al., *Shape Memory Alloys*, Ed. by Kh. Funakubo (Metallurgiya, Moscow, 1990).

2. Y. G. Song, W. S. Li, L. Li, and Y. F. Zheng, "The influence of laser welding parameters on the microstructure and mechanical property of the as-jointed NiTi alloy wires," Mater. Lett. **62**, 2325−2328 (2008).

3. Gong Wei-Huai, Chen Yu-Hua, and Ke Li-Ming, "Microstructure and properties of laser micro welded joint of TiNi shape memory alloy," Trans. Nonferrous Met. Soc. China **21**, 2044−2048 (2011).

4. P. Schlossmacher, T. Haas, and A. Schüssler, "Laser-welding of a Ni-rich TiNi shape memory alloy: mechanical behavior," J. Phys. IV France **7**, 5−252 (1997).

5. B. Tam, M. I. Khan, and Y. Zhou, "Mechanical and functional properties of laser-welded Ti−55.8 wt pct Ni nitinol wires," Metall. Mater. Trans. A **42**, August, 2166 (2011).

6. S. S. Mani Prabu, H. C. Madhu, S. Perugu Chandra, K. Akash, P. Ajay Kumar, V. Satish Kailas, Manivan-nan Anbarasu, and I. A. Palani, "Microstructure, mechanical properties and shape memory behaviour of friction stir welded nitinol," Mater. Sci. Eng., A (2017).

7. S. S. Mani Prabu, H. C. Madhu, S. Perugu Chandra, K. Akash, R. Mithum, P. Ajay Kumar, V. Satish Kailas, Manivannan Anbarasu, and I. A. Palani, "Shape memory effect, temperature distribution and mechanical properties of friction stir welded nitinol," J. Alloys Compd. (2018).

8. V. Delobelle, P. Delobelle, Y. Liu, D. Favier, and H. Louche, "Resistance welding of NiTi shape memory alloy tubes," J. Mater. Proc. Techn. **213**, 1139−1145 (2013).

9. Fox Gordon, Hahnlen Ryan, and J. Dapino Marcelo, "Fusion welding of nickel−titanium and 304 stainless steel tubes: Part II: tungsten inert gas welding," J. Intell. Mater. Systems Struct. **24** (8), 962−972 (2012).

10. F. A. Rodrigues Luiz, A. Amorim Fernando, F. R. Pereira Francisco, and J. de Araujo Carlos, "Experimental study of tungsten inert gas pulsed welding applied to Ni−Ti shape memory alloy wires," Mater. Res. Soc. Symp. Proc. **1765** (2015).

11. J. P. Oliveira, D. Barbosa, F.M. Braz Fernandes, and R. M. Miranda, "Tungsten inert gas welding of Ni-rich NiTi plates: functional behavior," Smart Mater. Struct. **25** (2016).